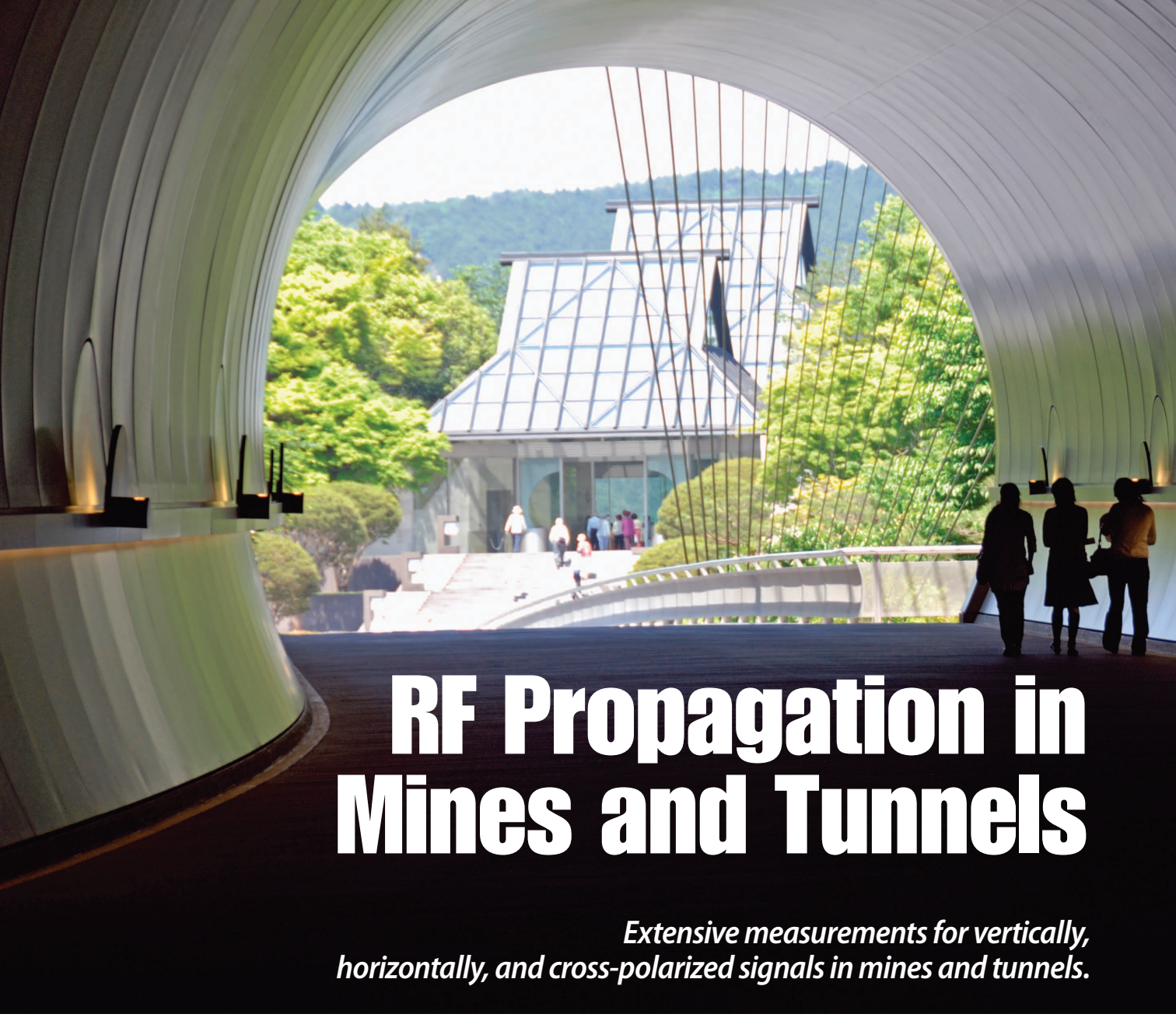

RF Propagation in Mines and Tunnels

Extensive measurements for vertically, horizontally, and cross-polarized signals in mines and tunnels.

Chenming Zhou, Timothy Plass, Ronald Jacksha, and Joseph A. Waynert

This article reports measurement results on radio-frequency (RF) propagation in tunnels and mines for vertically, horizontally, and cross-polarized signals. Extensive measurements have been made in concrete tunnels, coal mines with rock dust and shotcrete, with and without conductive mesh, and hard-rock mines. The measurements include power attenuation over distances with and without line of sight (LOS) at four frequencies (455, 915, 2,450, and 5,800 MHz) that are common to underground radios, as well as swept wideband-frequency measurements from 30 MHz to 1 GHz at fixed separation distances to investigate the attenuation behavior as the waveguide cutoff frequency is approached. In addition, power loss associated with radio propagation around a 90° corner was measured for the four frequencies and two polarizations in an operational coal mine.

The data show the importance of the tunnel dimensions, frequency, polarization, and electrical properties of the tunnel walls on the signal propagation characteristics. The propagation

Digital Object Identifier 10.1109/MAP.2015.2453881
Date of publication: 26 August 2015

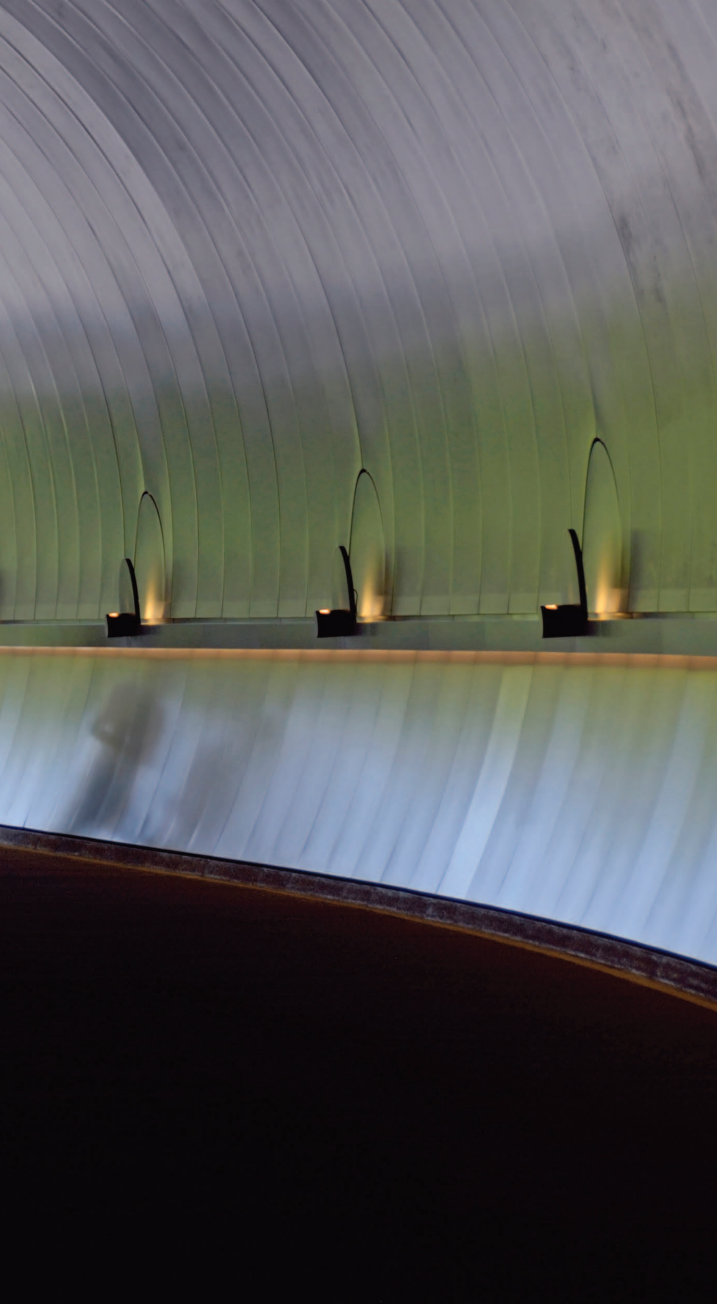

IMAGE LICENSED BY INGRAM PUBLISHING

Antenna polarization plays a more important role for tunnels that have a greater difference between their width and height.

measurements generally show a rapid power drop in the first 10–50 m (often referred to as the near zone) followed by a more gradual linear decrease (far zone) when plotted versus the separation distance.

We also show that the simulation results based on both the ray-tracing and modal methods match the measurement results in a straight concrete tunnel, indicating that propagation behavior in such a tunnel environment can be well modeled by the basic dielectric waveguide theory.

BACKGROUND

In response to a series of fatal underground coal mining disasters, the U.S. Congress passed the Mine Improvement and New Emergency Response (MINER) Act [1]. The MINER Act requires all U.S. underground coal mines to install wireless communication systems to provide communications between underground miners and surface personnel, especially during an emergency. Many coal mines have installed communication systems that use conventional radio frequencies in the ultrahigh-frequency (UHF) and superhigh-frequency bands. Frequencies of particular interest are 455 and 915 MHz, and 2.45 and 5.8 GHz, which are representative of those used in commercially available mine wireless communications and tracking systems.

UHF propagation in mines and tunnels differs significantly from that above ground, but previously the underground behavior was not fully understood or able to be accurately modeled. The National Institute for Occupational Safety and Health's (NIOSH) Office of Mine Safety and Health Research has been performing research on radio signals in mines to improve the understanding of and ability to accurately model UHF propagation in mines as a means to enhance both preaccident and postaccident performance of communications and tracking systems. Propagation measurements were made in uniform, straight concrete tunnels that could be easily modeled, as well as several coal and hard-rock mines with various dimensions, boundary materials, and assorted conductors. Measurements were made at four test frequencies for both vertically and horizontally polarized signals along the axial length of the tunnels. Cross-polarization combinations of propagation were measured in many of the test sites. Additional characterization of the signal propagation was performed using swept frequency measurements that enabled the computation of signal attenuation per 100 m as a function of frequency.

MEASURING PROPAGATION IN TUNNELS AND MINES: RELATED WORK

One of the earliest efforts of experimentally exploring radio propagation in tunnels took place in the 1920s when researchers in the U.S. Bureau of Mines (USBM) performed experiments to detect radio signals from inside the Pittsburgh experimental mine located in Pittsburgh, Pennsylvania [2]. Since then "tunnel talking" [3] has drawn significant attention, and numerous theoretical and experimental contributions have appeared in the open literature. Table 1 summarizes some existing measurement work in straight road or subway tunnels. In addition, some measurement campaigns were performed in curved tunnels, and the results were reported in [4]–[7].

In comparison with the many measurements reported involving road or subway tunnels, there have been relatively

TABLE 1. SOME EXAMPLES OF THE PUBLISHED MEASUREMENT WORK IN ROAD/SUBWAY TUNNELS.

Research Group	Year	Polarizations	Frequency (MHz)	Description
Chiba et al. [23] (Japan)	1978	HH, VV, and VH	40, 60.150, 470, 900, 1,700, and 4,000	A straight, concrete tunnel. The entrance is circular with a flat base.
Zhang et al. [24] (Singapore)	2000	VV	465 and 820	Quasi-straight; arch-shaped.
Didascalou et al. (Germany) [6]	2001	HH	945 and 1,853.4	A short, straight, rectangular, and wide profile tunnel section.
Wang and Yang (Taiwan) [5]	2006	HH and HV	943.4 and 942	Circular with a flat base; straight.
Lienard et al. (France) [4], [25]	2007	VV	450, 900, and 450–5,000	Circular with a flat base.
Masson et al. (France) [26]	2009	VV	2,400 and 5,800	Arch-shaped.

Note: "V" and "H" in the "Polarizations" column denote vertical and horizontal polarizations, respectively. The notation is defined in such a way that the first letter represents the polarization of the transmitting antenna and the second the receiving antenna. For example, "VH" represents the scenario that the transmitting antenna is vertically polarized and the receiving antenna is horizontally polarized. Unless stated otherwise, this polarization notation will be used in the rest of this article.

few reported measurement efforts in mines to date. The relative lack of experimental studies in mines is partially due to the difficulty in accessing operational mines. As a result, some researchers have chosen to build a scaled-down tunnel in the laboratory to experimentally study tunnel propagation mechanisms [8], [9]. Many other researchers rely on measurement results in the open literature to validate their proposed/developed models. For example, one of the earliest USBM-sponsored propagation measurements in coal mines at UHF and VHF [10] has been referenced by [11] and recently by [12] for validating their theoretical analyses. Aside from several early investigation reports supported by USBM [10], [13], [14], Zhang et al. [15] made some propagation measurements in two longwall coal mines in China at 900 MHz. French researchers Lienard and Degauque [16] measured underground mine channels both in the narrowband (150, 450, and 900 MHz) and wideband (400–500 MHz) [16]. Recently, many underground mine measurements were carried out at the Canada Centre for Mineral and Energy Technology mine [17]–[20] at frequencies of 2.4 and 5.8 GHz. In addition, radio propagation in long caves and subterranean galleries share some similarities with propagation in mines and have been reported in [21] and [22].

In this article, we report our extensive measurement results in different environments (including simple concrete tunnels, coal mines with rock dust and shotcrete, with and without conductive mesh, and hard-rock mines) at different frequencies (455, 915, 2,450, and 5,800 MHz) and with different polarizations (vertical, horizontal, and cross polarizations). In addition, the power loss associated with radio propagation around a 90° corner was measured for the same frequencies and polarizations in an operational coal mine.

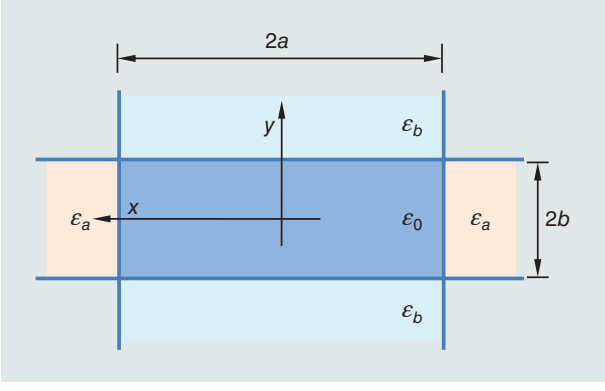

FIGURE 1. A cross section of the waveguide with four dielectric walls.

MODELING RF PROPAGATION IN MINES AND ITS CHALLENGES

We consider a straight hollow dielectric waveguide with rectangular cross-sectional dimensions 2b and 2a, as depicted in Figure 1. Let ε_0 denote the permittivity of air and $\varepsilon_{a,b}$ the complex permittivity of the vertical and horizontal walls surrounding the waveguide, respectively. The origin of the coordinate system is in the center of the waveguide cross section, with x horizontal, y vertical, and z down the waveguide. The magnetic permeability of all media is assumed to be the same and equal to that of the free space μ_0. A transmitter (Tx) is located at $T(x_0, y_0, 0)$ and a receiver (Rx) at $R(x, y, z)$. Without loss of generality, we also assume that the source is vertically polarized.

MODELING RADIO PROPAGATION IN TUNNELS AND MINES

RAY TRACING METHOD

Based on the ray-tracing method, the electric field in a hollow tunnel can be represented by a summation of the electric fields from the two-dimensional images of the source in the excitation plane, which is defined as the cross-sectional plane of the tunnel where the Tx lies. The coordinates of the image $I_{m,n}$ of an arbitrary point source located at $T(x_0, y_0, z_0)$ can be obtained as [27], [28]

$$x_m = 2ma + (-1)^m x_0$$
$$y_n = 2nb + (-1)^n y_0, \quad (1)$$

where integers m and n represent the number of reflections that the ray undergoes relative to the horizontal and vertical walls, respectively. The electric field at an arbitrary point $R(x, y, z)$ within the tunnel can be obtained as [27]–[30]

$$E_r(x, y, z) = E_t \sum_{m=-\infty}^{+\infty} \sum_{n=-\infty}^{+\infty} \frac{e^{-jkr_{m,n}}}{r_{m,n}} \rho_{\perp}^{|m|} \rho_{/\!/}^{|n|}, \quad (2)$$

where E_t is the transmitted electric field, k is the wave number in the waveguide, and $r_{m,n}$ is the distance between the Rx and the image $I_{m,n}$ and is given by

$$r_{m,n} = \sqrt{(x_m - x)^2 + (y_n - y)^2 + z^2}. \quad (3)$$

$\rho_{\perp,/\!/}$ represent the perpendicular and parallel reflection coefficients, respectively, and can be calculated as

$$\rho_{\perp,/\!/} = \frac{\cos\theta_{\perp,/\!/} - \Delta_{\perp,/\!/}}{\cos\theta_{\perp,/\!/} - \Delta_{\perp,/\!/}}, \quad (4)$$

where $\theta_{\perp,/\!/}$ is the incidence angle relative to a normal to the reflecting surface and is described by

$$\theta_{\perp} = a\cos(|x_m - x|/r_{m,n}) \quad \theta_{/\!/} = a\cos(|y_n - y|/r_{m,n}). \quad (5)$$

Here, $\Delta_{\perp,11}$ is a quantity related to the effective surface impedance defined as

$$\Delta_{\perp} = \sqrt{\bar{\varepsilon}_a - \sin^2\theta_{\perp}} \quad \Delta_{/\!/} = \sqrt{\bar{\varepsilon}_b - \sin^2\theta_{/\!/}}/\bar{\varepsilon}_b, \quad (6)$$

where $\bar{\varepsilon}_{a,b} = \varepsilon_{a,b}/\varepsilon_0$ are the relative permittivities of the vertical and horizontal walls, respectively.

MODAL METHOD

For the modal method, the electric field is written as [31], [32]

$$E_r = \frac{-j2\pi E_t}{ab} \sum_{p=1}^{+\infty} \sum_{q=1}^{+\infty} A_{p,q} \frac{e^{-(\alpha_{p,q} + j\beta_{p,q})z}}{\beta_{p,q}}, \quad (7)$$

where E_t is the transmitted electric field, and

$$A_{p,q} = \sin\left(\frac{p\pi}{2a}x + \varphi_p\right)\sin\left(\frac{q\pi}{2b}y + \varphi_q\right)\sin\left(\frac{p\pi}{2a}x_0 + \varphi_p\right)\times \sin\left(\frac{q\pi}{2b}y_0 + \varphi_q\right) \quad (8)$$

is the mode eigenfunction that reflects the influence of both the Tx and Rx antenna positions on the power distribution. In addition

$$\alpha_{p,q} = \frac{1}{a}\left(\frac{p\lambda}{4a}\right)^2 \mathrm{Re}\left\{\frac{1}{\sqrt{\bar{\varepsilon}_a - 1}}\right\} + \frac{1}{b}\left(\frac{q\lambda}{4b}\right)^2 \mathrm{Re}\left\{\frac{\bar{\varepsilon}_b}{\sqrt{\bar{\varepsilon}_b - 1}}\right\}$$
$$\beta_{p,q} = \sqrt{k^2 - \left(\frac{p\pi}{2a}\right)^2 - \left(\frac{q\pi}{2b}\right)^2} \quad (9)$$

are the propagation and attenuation constants, respectively. Here, $\mathrm{Re}\{\cdot\}$ denotes the real part of the argument. The two phase constants $\varphi_{p,q}$ are defined as

$$\varphi_{p,q} = \begin{cases} 0 & p(q) \text{ is even} \\ \pi/2 & p(q) \text{ is odd} \end{cases}. \quad (10)$$

THE EQUIVALENCE OF THE RAY-TRACING AND MODAL METHODS

For a perfectly electric conducting (PEC) waveguide, it is known that the ray-tracing method is equivalent to the modal method [33], [34]. Recently, Zhou and Waynert [31] have mathematically proved that the two methods are equivalent for a lossy dielectric tunnel. The major difference between modeling a PEC waveguide and a dielectric waveguide is the modal attenuation constant term shown in (9). As shown in [28], this modal attenuation constant is a direct result of the power loss caused by multiple reflections of waves/rays on the four tunnel walls and, therefore, is zero for PEC waveguides. It is shown in [31] that the classical modal attenuation constant can be derived based on the ray summation of the electrical field through a Poisson summation formula. It is also clearly illustrated in [31] that the existence of modal attenuation constants is mainly due to the fact that the reflection coefficients from the four tunnel walls are less than unity, so that part of energy is transmitted into the tunnel walls as the rays are reflected.

Although both (2) and (7) are based on a vertically polarized source, it is worth noting that the corresponding expression for the horizontal polarization can be readily obtained by switching associated variables. For example, for the ray-tracing method, the electric field expression in (2) corresponding to the horizontal polarization can be obtained by switching "x" to "y", "m" to "n", and "a" to "b" in (1) and (3)–(6). Note that a switch should be performed even when those symbols appear in the subscript. The switch operation can be explained by the relative rotation principle.

It should be noted that radio propagation in tunnels has been extensively investigated and several theoretical models have been proposed. It is our goal in this article to present a unified ray-tracing and modal solution with sufficient details so that other researchers can directly use them when needed. The main contributions of our unified modeling work as compared with other modeling work in the literature include the following:

- We provide a general analytical form for both the ray-tracing and modal methods. The general form incorporates all the major propagation controlling factors, which will be discussed in detail in the following section.
- We present a unified ray-mode solution for modeling tunnel propagation. The equivalence of the ray and modal methods is mathematically proved [31] under the condition of high frequencies and large Tx–Rx separation distances. The numerical results are provided to show that the two methods yield the same result.
- We validated the ray-tracing and modal methods with extensive measurement results in a real tunnel at four different frequencies and for two polarizations.

CONTROLLING FACTORS

DIMENSIONS

By a close examination of the attenuation constant in (9), we can find that the tunnel cross-sectional dimensions are the

most important parameters since the attenuation constant varies inversely with the cube of the dimensions, as compared with the square of the frequency and approximate square root of the complexity permittivity. A small change in tunnel dimensions leads to a significant change in the attenuation constant. Likewise, given a fixed system frequency and tunnel wall material, tunnels with a large cross-sectional area generally lead to a smaller attenuation constant. Conversely, for a fixed cross-sectional area, the attenuation constant varies with the exact shape of the cross section.

FREQUENCY

There are generally two types of losses related to system frequency: the antenna loss and the waveguide loss. The antenna loss is the inherent power loss caused by its radiating element. It is caused by the frequency dependency in the antenna aperture formulation and is also the source of the frequency dependency in the well-known Friis transmission equation corresponding to the free space environment. The antenna loss is unavoidable since an antenna is always needed to transmit or receive RF signals in a wireless communication system. It is, however, a fixed value for a fixed frequency and independent of the separation distance, given that the distance is larger than one wavelength.

The second type of loss is the waveguide (propagation) loss that is characterized by the attenuation constant in (9). Unlike the antenna loss, the propagation loss is proportional to distance. In addition, based on (9), it is evident that the propagation loss (in decibels per meter) in a straight tunnel is inversely proportional to the square of the frequency.

When the frequency increases, the antenna loss increases, but the propagation loss decreases. Therefore, a tradeoff is needed when one tries to search for the optimum frequency (minimum loss) in a tunnel environment. In general, depending on the geometric conditions of the tunnel, high-frequency signals are better for long-range communication since the associated propagation loss is less at higher frequencies, although they suffer from a large one-time loss when the signals are radiated and received by antennas.

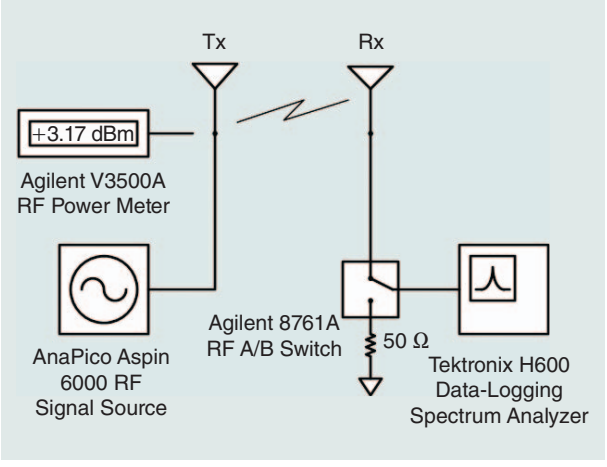

FIGURE 2. The RF test apparatus block diagram.

POLARIZATION

It is apparent that in narrow and high tunnels where $a < b$, vertically polarized signals attenuate less compared with horizontally polarized signals. The opposite is true for wide and low tunnels where $a > b$. In general, to achieve the minimum loss in a rectangular tunnel, the polarization of the *E*-field should coincide with the larger transverse dimension of the tunnel.

ELECTRICAL PROPERTIES

As shown in (9), the impact of the tunnel complex permittivity on the attenuation constant is relatively small compared with the frequency and tunnel dimensions since the attenuation constant approximately varies with the square root of the permittivity.

ANTENNA POSITION

As shown in (8), the power distribution in a tunnel is also affected by the position of the transmitting and receiving antennas relative to the tunnel walls. In general, positions close to the center of the tunnel are more favorable in terms of the system power compared with positions close to any of the four walls. Unfortunately, mounting antennas in a center position is not practical as antennas may obstruct or interfere with the traffic. Therefore, antennas are generally mounted near the wall even though doing so will result in additional power loss from a radio-propagation perspective.

MEASUREMENT SETUP

The design for the RF test apparatus was driven by the unique environment of an underground coal mine. Ruggedness, portability, and simplicity were the goals: a system able to survive the harsh environment of an operating underground mine yet still be easily broken down for transport and quickly set up for measurements. Materials such as polyvinyl chloride (PVC), carbon fiber, plastic, and plywood were used whenever possible in an effort to keep the measurement system RF transparent. Finally, all the instruments were required to be battery powered due to the limited availability of mains power in the test areas.

The block diagram of the test apparatus is shown in Figure 2. It is composed of two components: a stationary Tx and a mobile Rx. The Tx consists of an AnaPico ASPIN 6000 RF signal source connected to one of four omnidirectional J-pole antennas (Laird FG4500, Laird FG8960, Laird FG24005, or SuperPass SPDJ40) for RF propagation measurements or one of three biconical antennas for swept frequency measurements (A.H. Systems SAS-542, A.H. Systems SAS-542F, or A.H. Systems SAS-545). For RF propagation measurements, the Rx consists of a Tektronix H600 data-logging spectrum analyzer connected through an Agilent 8761A RF A/B switch to either a 50-Ω termination or an antenna matching that of the Tx. For swept RF measurements, the A/B switch and the Tektronix spectrum analyzer were replaced with an Anritsu MS2036C spectrum analyzer connected directly to an antenna matching that of the Tx.

Figure 3 is a picture of the test apparatus. On the right is the Tx with an antenna shown mounted in vertical polarization on a carbon fiber antenna stand and connected to the RF source with an LMR-400UF coaxial cable. On the left is the cart used for Rx

mobility. It was constructed of plywood with plastic wheels and a PVC handle which allowed the operator to be approximately 2 m in front of the antenna during the measurements. Similar to the Tx, an antenna is also shown mounted in vertical polarization on a carbon fiber antenna stand and connected to the spectrum analyzer with an LMR-400UF coaxial cable.

RF signal propagation was measured as follows. The RF signal source was configured to produce a continuous wave signal with a fixed output power. An Agilent V3500A RF power meter was used to verify power at the Tx antenna end of the coaxial cable before the beginning of each propagation measurement. The spectrum analyzer was configured to measure channel power with its input connected to the 50-Ω termination through a microwave A/B switch. To begin a measurement, data logging was started on the spectrum analyzer, its input was switched to the Rx antenna, and the mobile Rx cart was pulled away from the Tx. At presurveyed intervals of distance—typically, 30 m—the mobile Rx cart was halted and the spectrum analyzer's input was momentarily switched to the 50-Ω termination. This inserted a received power null in the measured data that served as a distance indicator. The spectrum analyzer's input was then switched back to the Rx antenna, and travel away from the Tx was resumed. Postprocessing of the logged data was performed to correlate the power nulls in the data to the presurveyed distances.

Unless stated otherwise, the height of the transmitting and receiving antennas was set to 1.22 m. The Tx and Rx were placed in the center line of the tunnel.

Swept frequency measurements were made as follows. Using sets of A.H. Systems biconical antennas for both the Tx and Rx, the RF signal source was configured to sweep frequency at a constant power level while the spectrum analyzer was configured to sweep the same frequency range in peak trace hold mode. At presurveyed fixed intervals of distance—typically 3 or 15 m—measurements were made and the spectrum analyzer trace data saved. Postprocessing of the data determined the incremental change in the RF signal level over distance. These increments were averaged to produce curves of attenuation per 10 m as a function of frequency.

RESULTS

STRAIGHT CONCRETE TUNNEL WITH SMOOTH WALLS

To gain some basic understanding about tunnel propagation, we started the measurements with a relatively simple case: a straight concrete tunnel with smooth walls. We measured power attenuation along a 610-m section of the concrete tunnel illustrated in Figure 4.

Comparisons between the simulated and measured propagation results at different frequencies are shown in Figures 5 and 6 (for the horizontal and vertical polarization, respectively). In Figures 5 and 6, the solid blue line represents the measured result, and the green dashed and red dashed-dotted lines denote the mode- and ray-based simulation results, respectively. The tunnel has an arched ceiling, but we approximated the cross section of the tunnel as a rectangle with the same width and an effective height of 2.35 m in our model. The same electrical properties ($\bar{\varepsilon}_{a,b} = 8.9$ and $\sigma = 0.15$ S/m) are used for all four frequencies and the four tunnel walls. It is shown that the ray-tracing and modal methods yield the same simulation results, which agree with the measurement results for all four frequencies and for both polarizations. The excellent agreement between the simulated and measured power confirm that the radio propagation in tunnels can be well described by both the ray-tracing and modal methods.

Both the simulation and measurement results in concrete tunnels show that propagation can be divided into two

FIGURE 3. The RF test apparatus.

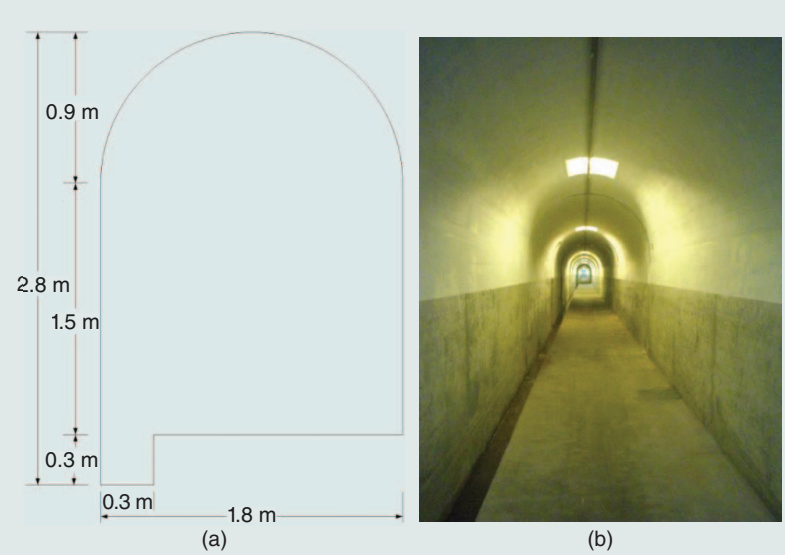

FIGURE 4. (a) The geometry of a straight concrete tunnel with arched ceiling and smooth walls and (b) a photograph of the tunnel.

regions: the near and far zone. The signal power fluctuates widely in the near zone and attenuates linearly with the distance in the far zone. The propagation behavior in the two zones can be easily interpreted based on waveguide (modal) theory. As shown in (9), the modal attenuation constants for higher-order modes are significantly greater than the lowest mode $EH_{1,1}$. As a result, after a sufficiently long distance, all the higher modes will be strongly attenuated, and only the lowest mode remains. In this case, the propagation behavior is mainly dominated by the lowest mode, which is also referred to as the dominant mode. Based on modal theory, the rapid fluctuations in the near zone are caused by the interaction of higher-order modes with the dominant mode, and the quasi-linear behavior in the far zone is an indication of the single mode (the dominant mode) propagation. The point separating the near and far zone is known as the Fresnel zone breaking point [4], [35]–[38]. The breaking point is generally related to the system wavelength and tunnel dimensions. It moves closer to the Tx as the frequency decreases. It is also observed that the attenuation rate in the far zone increases as the frequency decreases. As a result, the signal power attenuates very quickly at 455 MHz and reaches the noise floor power level (about −120 dBm) of the equipment after a short distance, causing the measured power curve to remain flat over the distance, as can be observed in Figure 6(a).

OLD SHOTCRETE-LINED COAL MINE

RF propagation measurements were made in a 335-m section of a mine at the Pittsburgh experimental mine, which is an inactive shotcrete-lined coal mine located in the Pittsburgh suburb of Bruceton, Pennsylvania. It is the same mine where the very early RF tunnel propagation tests were made by the USBM in 1921 [2]. The width and height of the entry (tunnel) vary with the axial distance, but, on average, the tunnel is about 3 m high and 2 m wide. Significant roughness has been observed on all four walls of the tunnel. The measurements performed were of two types. First, signal-level measurements were taken every 0.3–0.6 m along the tunnel length using a fixed frequency with horizontal, vertical, and cross polarization at 455 and 915 MHz, and 2.45 and 5.80 GHz. The second type of measurement used lower-frequency sweeps from a Tx that was monitored with a spectrum analyzer and a receive

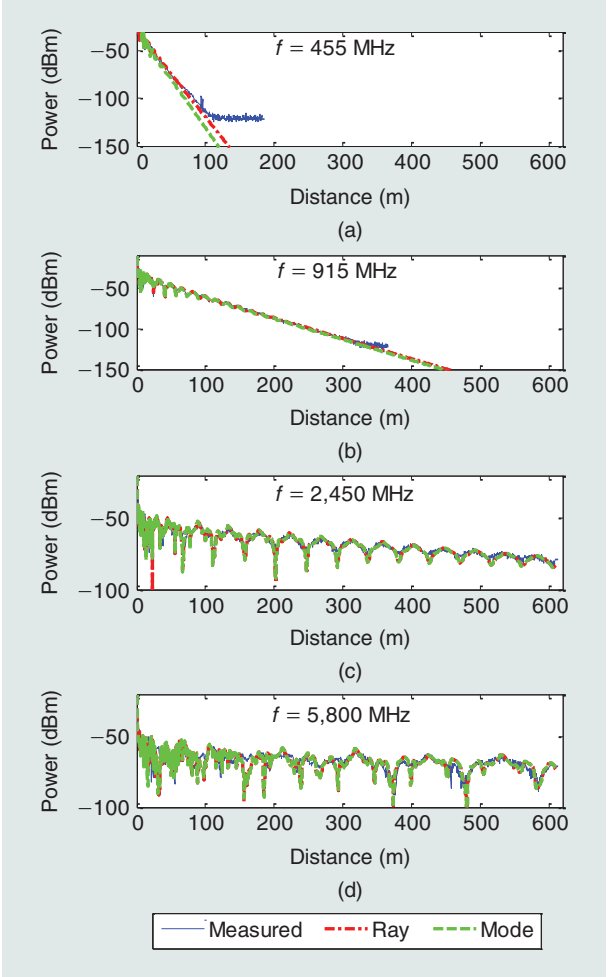

FIGURE 5. (a)–(d) The measured and simulated power attenuation over distance in a concrete tunnel (horizontal polarization).

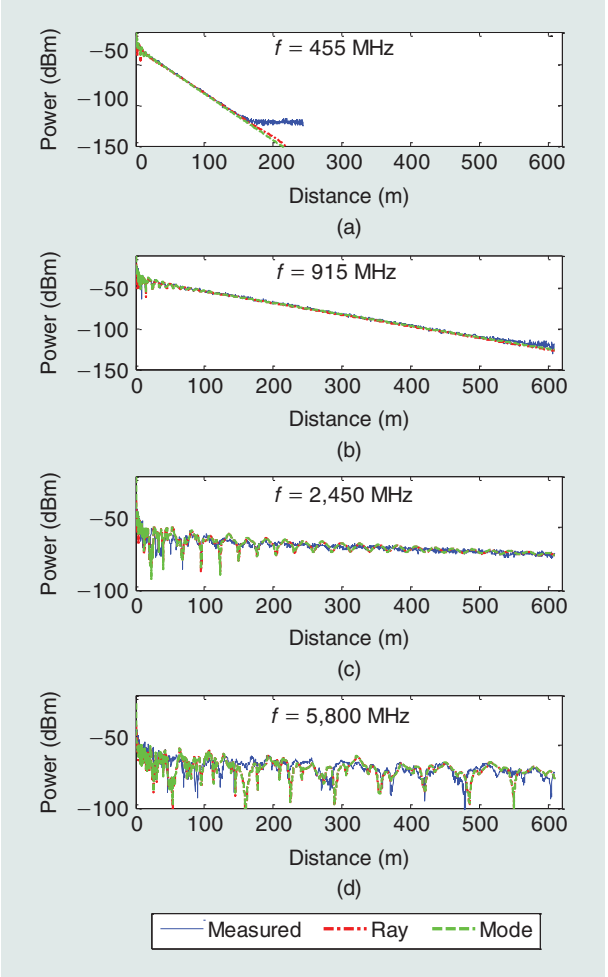

FIGURE 6. (a)–(d) The measured and simulated power attenuation over distance in a concrete tunnel (vertical polarization).

antenna that was moved in 3-m increments to determine the signal drop-off. Figure 7 shows the entrance of the mine [Figure 7(a)] and the experimental setup [Figure 7(b)] for the sweep measurements (the second type of measurement) inside the mine.

Figure 8 shows the propagation measurement results in the Pittsburgh experimental mine. Again, we use the same polarization notation as in Table 1. The linear signal attenuation in the 455- and 915-MHz measurements is apparent in these plots. The reason linear attenuation does not show in the 5.8-GHz plot is that the tunnel is relatively short. We expect the linear attention to appear if the tunnel and measurements are extended to a sufficiently long distance.

For all the four measured frequencies, it is found that HH polarization gives the minimum attenuation, which can be explained by the fact that the tunnel's horizontal dimension is greater than its vertical dimension.

Another interesting observation from these plots (especially from the 415- and 915-MHz plots) is that the cross-polarization signals (HV and VH) eventually show a slope similar to the HH signal after a sufficiently long separation distance, although they are about 20 dB lower than the copolarization signal HH. This indicates that the vertical antenna is measuring the

FIGURE 7. An RF propagation measurement in the Pittsburgh experimental mine: (a) the entrance of the mine and (b) the experimental setup for the sweep measurements (the second type of measurement) inside the mine.

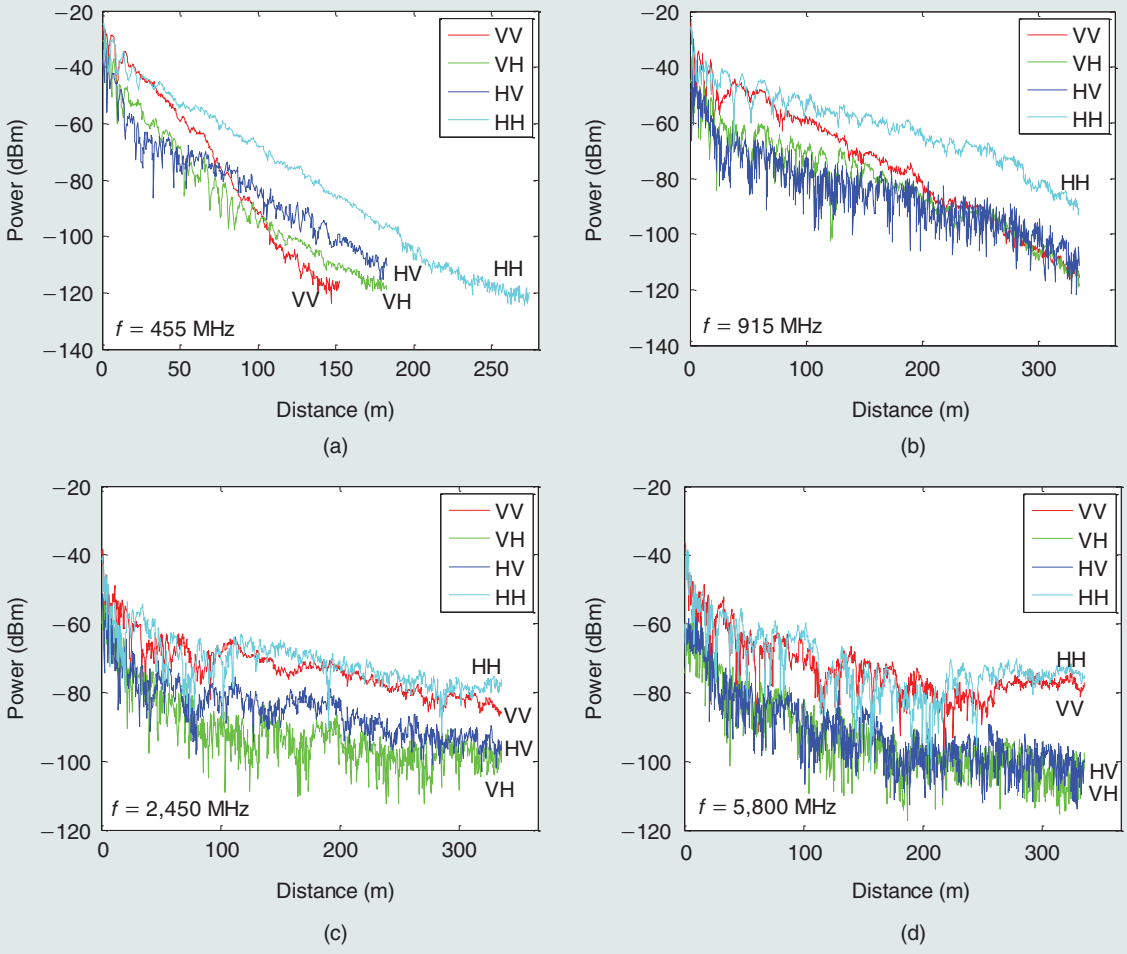

FIGURE 8. The propagation measurement results in the Pittsburgh experimental mine at (a) 455 MHz, (b) 915 MHz, (c) 2,450 MHz, and (d) 5,800 MHz.

horizontal signal but with −20 dB of cross-polarization isolation. In the 915-MHz plot, the VV signal shows a slope similar to the HH signal after about a 200-m distance. This is probably due to the severe attenuation of the vertical component. It may well be that the original vertical transmission has a small horizontal component that is 25 dB below the vertical component (e.g., due to a poor antenna polarization isolation or if the antenna is mounted slightly off from the vertical axis with a small offset angle). After 200 m, the vertical component has been severely attenuated, and its power is even less than the horizontal component. In other words, the opposite polarization signal could simply be the remnants of the originally transmitted signal that becomes dominant at greater distances due to its lower attenuation in the tunnel. Similar cross-polarization phenomena were observed in an arched road tunnel with relatively larger dimensions in [25].

The second type of measurement performed in the tunnels was of frequency sweeps using biconical antennas. The setup is shown in Figure 7(b). The Tx and antenna were set up in the same fixed location used for the propagation tests. The Tx swept from 30 to 1,000 MHz in 3,001 discrete steps. The Rx was a second biconical antenna with the same polarization but connected to a spectrum analyzer with a trace set to peak hold to capture the maximum at each frequency of the swept Tx. The Rx is moved away from the Tx, and then the power loss for each discrete frequency component is measured. The tests were repeated by moving the Rx in 3-m increments from 15.2 to 45.7 m, then in 15.2-m increments from 45.7 to 228.6 m. These measurements enabled the collection of signal levels at each location for all the frequencies of the sweep. The higher frequencies are attenuated less over distance so that the increment is increased to provide useful measurements. The small increments are required for the lower frequencies since the power decrease into the noise floor of the instrumentation quickly. Using these data, the difference in signal levels for each frequency was determined at each Rx position. These measurements enabled the determination of the attenuation slopes at each frequency. The average slopes can then be plotted to show attenuation per 100 m over the measured frequency range.

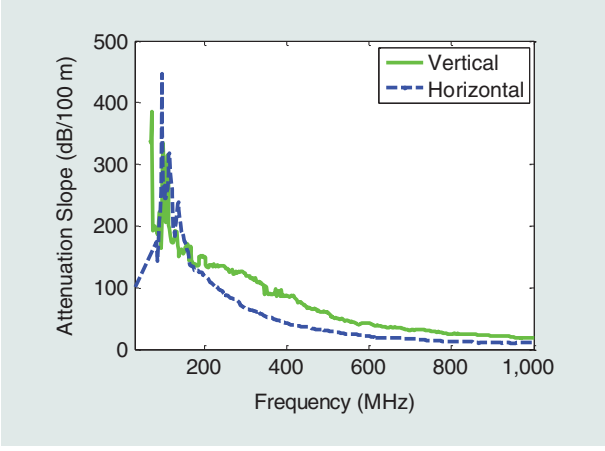

FIGURE 9. The measured wideband signal attenuation constants.

FIGURE 10. Conducting the propagation measurements in the hard-rock mine.

Figure 9 shows the measured attenuation slopes for the horizontal and vertical polarizations. As expected, for high-frequency signals, the horizontal polarization has a lower attenuation than the vertical polarization because the tunnel width is greater than the height. However, at the low end of the measured frequencies, we found that the vertical polarization actually has a lower attenuation. Thus, the vertical and horizontal polarization attenuation curves cross at a frequency of around 160 MHz. This is an interesting observation for low-frequency signals since it cannot be explained by classical waveguide theory, which assumes that the frequency of interest is sufficiently high such that the tunnel is electrically large. In addition, some large fluctuations in the measured attenuation slope at low frequencies are observed in Figure 9. This is probably due to the poor measurement accuracy at those low frequencies where signals attenuate so quickly with the distance.

HARD-ROCK MINE WITH QUASI-SQUARE CROSS DIMENSIONS

Propagation measurements were conducted along a 305-m section of a straight drift in a hard-rock silver mine, as shown in Figure 10. The cross-sectional dimensions of the mine were approximately 2.7 m high by 3.0 m wide, although they varied significantly (about ±0.5 m) along the test route as the surfaces were very rough. The tunnel was cut into the rock leaving rough rock walls and ceiling. The floor was very wet, with standing water in most places. The tunnel had steel mesh bolted to the ceiling and halfway down the walls. A significant amount of additional metal was present, including floor tracks, beams along the wall, roof bolts, a conduit, and water pipes near the ceiling. Again, we measured four frequencies (455, 915, 2,450, and 5,800 MHz), and the transmit power was set to the same level for all four frequencies.

Figure 11 shows the measurement results for 455 and 2,450 MHz for both the vertical and horizontal polarizations and Figure 12 for 915 and 5,800 MHz. In Figures 11 and 12, signals at higher frequency experience a significantly higher attenuation in the near zone. The higher attenuation for the higher-frequency signals is mainly due to the antenna loss (as discussed in the

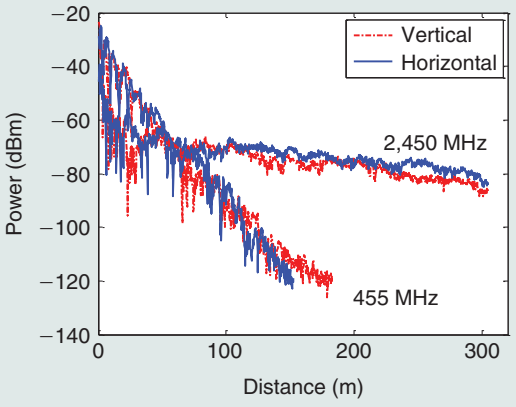

FIGURE 11. The propagation measurement results in the hard-rock mine (455 and 2,450 MHz).

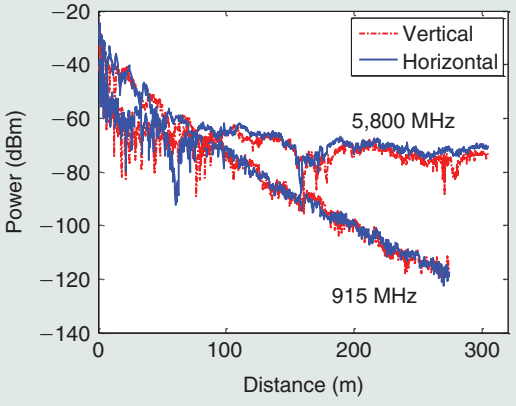

FIGURE 12. The propagation measurement results in the hard-rock mine (915 and 5,800 MHz).

"Modeling RF Propagation in Mines and Its Challenges" section), which is proportional to square of the frequency. The linear signal attenuation slopes that characterize the waveguide loss are apparent in these plots in the 455- and 915-MHz measurements. Again, the lowest frequency (455 MHz) gives the steepest attenuation slope, while the highest frequency (5,800 MHz) yields the minimum attenuation slope.

Another interesting observation from Figures 11 and 12 is that the slopes for the horizontal and vertical polarizations at the same frequency are similar. This is expected since the height and width of the tunnel are comparable. A more detailed explanation for this observation will be provided in the "Discussion" section.

WIDE EASTERN COAL MINE

RF propagation measurements were made in a 360-m section of an operational mine, our first opportunity to perform propagation tests in a long entry with a low ceiling and the large widths typically found in eastern coal mines. The entry did not contain any significant conductors, just isolated roof bolts and occasional metal straps between the roof bolts. There were no metal floor tracks, pipes, air ducts, ceiling mesh, or cables to influence the RF propagation in the coal walls, floor, and ceiling.

FIGURE 13. The mine entry of the wide eastern coal mine.

As shown in Figure 13, the tunnel selected for the tests had a ceiling about 1.7–2.0 m high and a width of approximately 6 m. The cross-sectional dimension of the entry varies (on the order of at least 0.3 m) with the axial distance. The entry was cut into the coal seam, leaving coal walls with a mostly shale rock ceiling and wet-clay floor. There were periodic perpendicular cross-cut tunnels of the same dimensions, leaving 6-m-wide side openings at 30-m intervals with 24-m square coal pillars. The walls were rough and uneven, with as much as 0.3-m variation from floor to ceiling along the length of the tunnel. Most of the wall surface was rock dust over broken coal, which forms random facets with small reflective surfaces. The floor was uneven, with 0.5–1.5-m variations in height along a 30-m section between coal pillars. The ceiling had roof bolts installed somewhat randomly but spaced at approximately 3-m increments, sometimes with 15-cm-wide metal strips going most of the way across the width of the entry. LOS was not always available due to the undulation of the mine tunnel.

The RF propagation tests were made with the cart moving down the center of the tunnel and its antenna height set to approximately 1.22-m above the floor, the same height as the Tx antenna. A single frequency and antenna polarization was

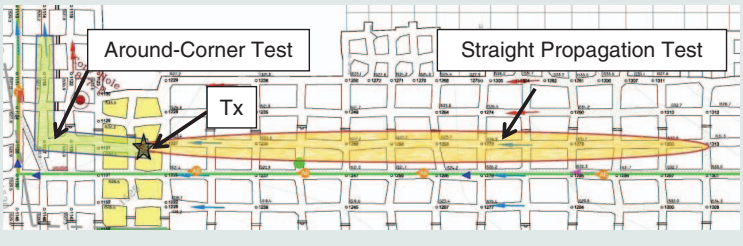

FIGURE 14. The mine map for the around-corner test and propagation test in a wide eastern coal mine.

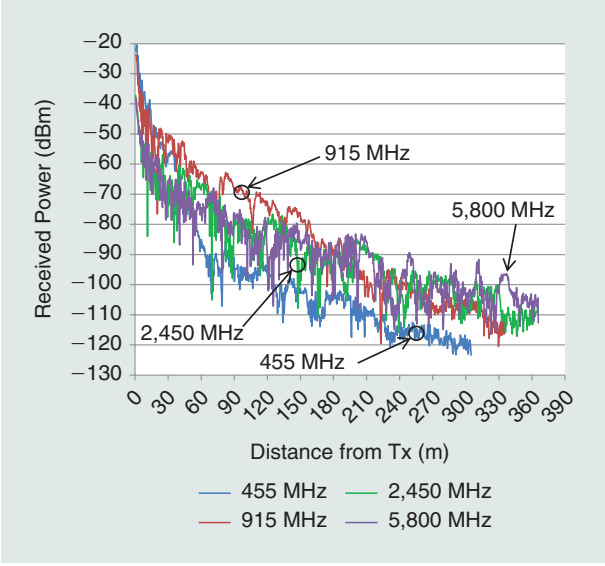

FIGURE 15. The propagation test results in the wide eastern coal mine (vertical polarization).

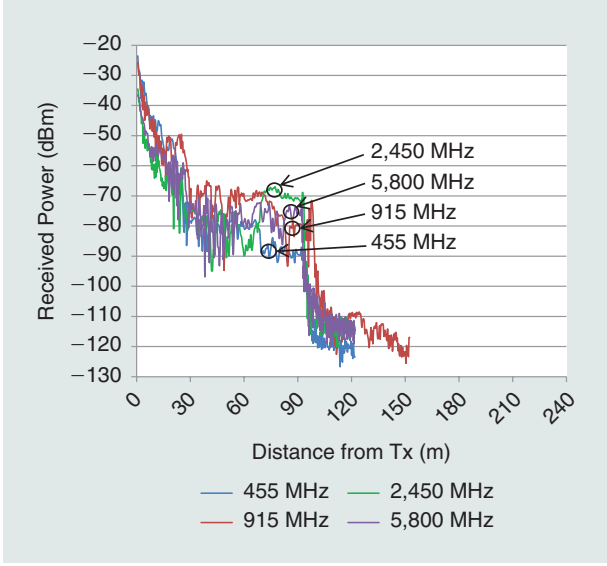

FIGURE 17. The around-corner propagation measurement results in the wide eastern coal mine (vertical polarization).

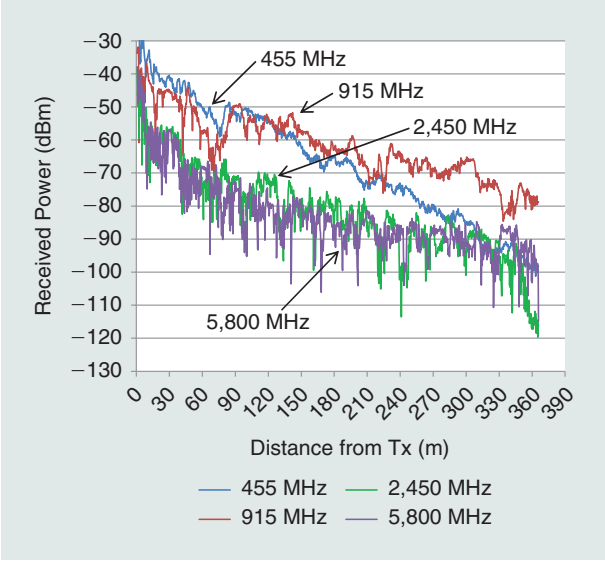

FIGURE 16. The propagation test results in the wide eastern coal mine (horizontal polarization).

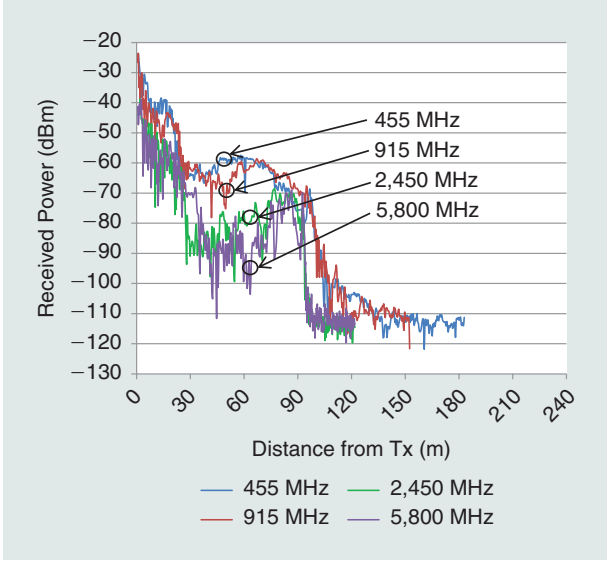

FIGURE 18. The around-corner propagation measurement results in the wide eastern coal mine (horizontal polarization).

configured for each measurement. The four frequencies, 455 and 915 MHz, and 2.45 and 5.80 GHz, were each tested with both horizontal and vertical polarizations. The test areas are marked in Figure 14 by an ellipse. The measurement results are shown in Figures 15 and 16.

The around-corner propagation test was made while approaching a 90° turn at 90 m from the Tx, continuing another 30–60 m along the far side of a coal pillar. The Tx was kept in the same location as in the previous tests (labeled as a star in Figure 14), but the cart was pulled toward the opposite direction (left in Figure 14) until it approached and turned the corner. Again, four frequencies were measured, and the results are shown in Figures 17 and 18 for vertical and horizontal polarizations, respectively. One obvious change in these plots is the abrupt drop in the signal level after the 90° turn is made at around 90 m. All frequencies attenuate to nearly the equipment noise floor after the turn, but the 455 and 915 MHz do not drop as precipitously and the horizontal signals do not appear to drop as much as the vertically polarized signal. This could be due to the fact that the horizontal signals are stronger going into the corner because of the wide width of the tunnel not attenuating them as much as the vertically polarized signal.

HIGH-ROOF WESTERN COAL MINE

RF propagation measurements were made in a 400-m section of a western coal mine. It was an opportunity to perform UHF

propagation tests in a long entry with a higher ceiling and the large widths typically found in western coal mines. The entry selected for the tests is in fresh air near the main access but is not a working entry. The entry, measuring 2.1–2.7 m high with a width of approximately 6 m, was cut into the coal seam, leaving a mostly coal floor and ceiling. It had perpendicular crosscut tunnels of the same dimensions from the right side only, leaving 6-m side openings at 30-m intervals, and 24-m square coal pillars. The left side was almost a continuous wall with few cutouts. The walls were rough and uneven, with as much as a 0.3-m variation from floor to ceiling and along the length. Most of the wall surface had light rock dust over broken coal, which formed random facets with small reflective surfaces. The entry contained conductors, including roof bolts, metal mesh on the ceilings and upper walls, and occasional metal straps between the roof bolts. There were no metal floor tracks, pipes, or air ducts, but there were large flexible water pipes and hoses on the floor and pallets of metal brackets in the center at around the 115-m distance.

Again, we measured the propagation power loss along the entry for four frequencies and both polarizations. The measurement results are shown in Figures 19 and 20 for vertical and horizontal polarizations, respectively. It is apparent in Figure 19 that the 455-MHz signal shows a significantly higher attenuation rate compared with the other frequencies. For Figures 19 and 20, the 455- and 915-MHz signals show a higher receive power than the 2.45- and 5.8-GHz signals for small separation distances, e.g., within 50 m. Since the transmitted power is the same for all the frequencies, the higher received power for lower-frequency signals at short separation distance results because high-frequency signals suffer from a higher loss caused by the antenna itself, as discussed in the "Modeling RF Propagation in Mines and Its Challenges" section. As the separation distance increases, the received power associated with high-frequency signals tends to have a lower attenuation rate. After a sufficiently long distance, the received power of the high-frequency signals is higher than that of the lower-frequency signals despite the initial larger power loss they experience due to the antennas.

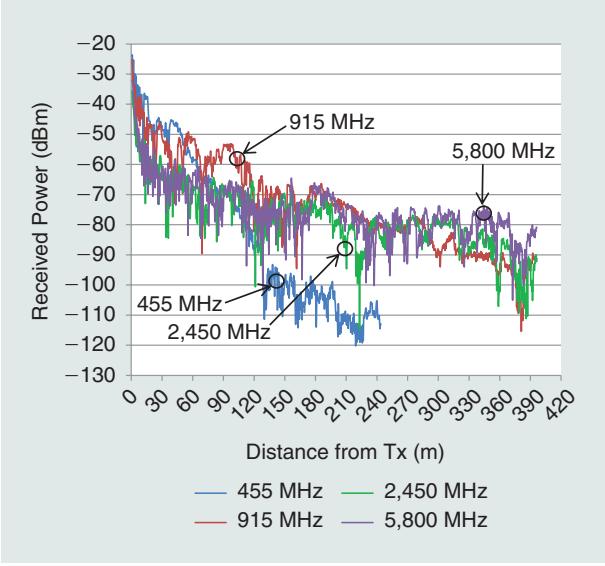

FIGURE 19. The propagation measurement results in the high-roof western coal mine (vertical polarization).

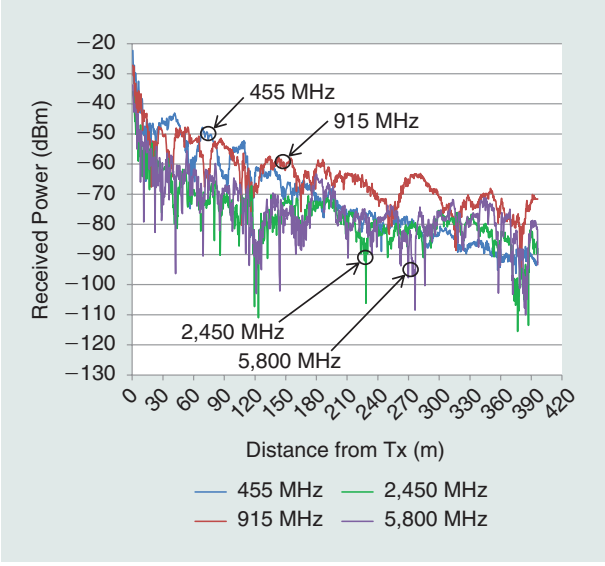

FIGURE 20. The propagation measurement results in the high roof western coal mine (horizontal polarization).

DISCUSSION

It should be noted that the concrete tunnel (Tunnel 1 in Table 2) reported in this article is a typical gallery in the Grand Coulee Dam in the state of Washington. It is different from typical road or subway tunnels reported in the literature in the sense that it has significantly smaller cross-sectional dimensions. For example, the road tunnel reported in [4] has an equivalent cross-sectional dimension of 7.8 m by 5.3 m, which is about ten times the cross-sectional area of the tunnel reported in this article. By comparing the results in this article to the results reported in [4], one may notice that the linear propagation behavior starts at a smaller separation distance in the smaller tunnel for the same frequency. For example, the linear attenuation behavior is apparent in Figures 5 and 6 for frequencies of 455 and 915 MHz within the first 200 m, while it does not fully appear even at the end of the tunnel (>2,500 m) in [4]. The linear attenuation behavior starting at a smaller distance for smaller tunnels can be explained by the modal theory introduced in the "Modeling RF Propagation in Mines and Its Challenges" section. Based on (9), the attenuation slope difference between the dominant mode and any higher modes $\mathrm{EH}_{p,q}$ can be expressed as

$$\Delta\alpha_{\mathrm{mod}\,e} = \alpha_{p,q} - \alpha_{1,1} = \frac{(p^2-1)\lambda^2}{16a^3}\mathrm{Re}\left\{\frac{1}{\sqrt{\bar{\varepsilon}_a - 1}}\right\} + \frac{(q^2-1)\lambda^2}{16b^3}\mathrm{Re}\left\{\frac{\bar{\varepsilon}_b}{\sqrt{\bar{\varepsilon}_b - 1}}\right\}. \quad (11)$$

It is apparent that the attenuation slope difference in (11) increases as the cross-section dimensions a and b decrease. In

other words, higher-order modes diminish faster for tunnels with small cross-sectional dimensions, and, thus, the dominant mode shows its dominance at a smaller distance.

The measurement data reported in [4] have been used by a variety of researchers for validating different theoretical models (e.g., in [30] and [39]). The measurement data (for Tunnel 1) reported in this article should be useful in the sense that it provides a more complete data set (by including four frequencies with both vertical and horizontal polarizations) for a model validation purpose. Moreover, compared with the road tunnels reported in the literature, Tunnel 1 reported in this article has very smooth and uniform walls, which makes it ideal for validating tunnel propagation models.

Comparing the measurement results at different frequencies for the same tunnel (Figures 5, 6, 8, 11, and 12) shows that the linear attenuation behavior for high-frequency signals starts at a greater separation distance. This can also be explained by (11). For the same tunnel with fixed dimensions, (11) implies that the attenuation rate difference between the dominant mode and higher modes decreases as the system frequency increases. Therefore, a greater distance will be needed for higher-mode signals to be attenuated to a negligible value compared with the dominant mode.

Radio propagation in tunnel environments is mainly characterized by its attenuation slope. In Table 2, we summarize the estimated attenuation slopes for the four frequencies and two polarizations in the different testing sites. The attenuation slopes are estimated at large distances from the measured power measurement results based on the method of linear regression fitting. As a result, the attenuation slopes in Table 2 can be viewed as the measured attenuation constants of the dominant mode $\alpha_{1,1}$ for different configurations in different tunnels. It should be noted that some estimated slopes associated with high-frequency signals such as 5.8-GHz signals might not be accurate because the maximum separation distances measured are not large enough to fully show the linear attenuation behavior.

As a cross check, the estimated attenuation rate in Tunnel 3 at 455 MHz is 66.7 and 35.2 dB/100 m for vertical and horizontal polarizations, respectively. The linear slopes at 915 MHz are 22.0 and 10.7 dB/100 m for vertical and horizontal polarizations, respectively. Those values are consistent with the values shown in Figure 8, which were measured through a different approach (wideband frequency sweeping test).

In Table 2, the attenuation slopes measured for Tunnel 3 are relatively close to the slopes measured in the concrete tunnel for the Grand Coulee Dam (Tunnel 1), although the horizontal and vertical results are reversed because Tunnel 1 is about 1.8 m wide and 2.4 m tall, compared with Tunnel 3 dimensions of about 3 m wide and 2 m tall. The slightly larger dimensions of Tunnel 3 are the reason for its slightly lower slope values.

Some analyses related to propagation controlling factors are given in the "Modeling RF Propagation in Mines and Its Challenges" section based on the modeling work introduced in the same section. After a comparison of the attention slopes given in Table 2, one will find that the analyses given in the "Modeling RF Propagation in Mines and Its Challenges" section are well supported by the measurement results in Table 2. For example, if we compare the attenuation slopes in Table 2 in the same tunnel/mine for the same polarization, it is apparent that the attenuation slope decreases with the frequency. In addition, if we compare the attenuation slopes in the same tunnel for the same frequency, we can find that the polarization coinciding with the larger transverse dimension of the tunnel gives less attenuation.

TABLE 2. A SUMMARY OF THE MEASURED ATTENUATION SLOPES IN DIFFERENT MINES/TUNNELS.

Index	Testing Sites	$W \times H$ (m)	455 MHz		915 MHz		2,450 MHz		5,800 MHz	
			Vertical Slope dB/100 m	Horizontal Slope dB/100 m	Vertical Slope dB/100 m	Horizontal Slope dB/100 m	Vertical Slope dB/100 m	Horizontal Slope dB/100 m	Vertical Slope dB/100 m	Horizontal Slope dB/100 m
1	Concrete tunnel	1.8 × 2.4	56.48	77.83	14.16	25.06	2.03	3.67	1.86	1.49
2	Pittsburgh experimental coal mine	2.2–4.0 × 1.8–2.3	67.32	35.22	22.61	12.1	7.42	7.81	N/A	N/A
3	Hard-rock coal mine	3.0 × 2.4–2.7	50.7	55.7	28.45	26.8	6.44	5.21	3.56	2.18
4	Wide eastern coal mine	6.1 × 1.7–2.0	107.79	16.37	19.9	8.15	12.25	8.48	10.65	6.26
5	High-roof western coal mine	6.1 × 2.1–2.7	51.49	12.16	11.62	6.86	6.91	5.04	4.42	4.34

A closer look at the VV and HH signals in the four plots shown in Figure 8 shows that the two signals exhibit significantly different propagation behaviors at 455 MHz but only a negligible difference at 5.8 GHz. In other words, the propagation difference caused by different polarizations decreases as the frequency increases. This can be also explained by the modal method introduced in the "Modeling RF Propagation in Mines and Its Challenges" section. Based on (9), assuming $\bar{\varepsilon}_a = \bar{\varepsilon}_b = \bar{\varepsilon}$, we can write the difference of the attenuation constants corresponding to the dominant mode of the vertical and horizontal polarizations as

$$\Delta\alpha_{\text{polarization}} = \alpha_{1,1}^{H} - \alpha_{1,1}^{V} = \frac{\lambda^2 \text{Re}\{\sqrt{\bar{\varepsilon}-1}\}}{16}\left(\frac{1}{a^3} - \frac{1}{b^3}\right). \quad (12)$$

From (12), it is apparent that as the wavelength decreases, the difference in the attenuation constant between the vertical and horizontal polarizations significantly decreases (changing with the square of the wavelength), given fixed tunnel dimensions (a and b).

In addition to the frequency dependency, it is also shown in (12) that the propagation difference associated with signal polarization is mainly caused by the difference in the cross-sectional dimensions. For a square cross-sectional dimension where $a = b$, we have $\Delta\alpha_{\text{polarization}} = 0$. As a result, the propagation difference between the vertical and horizontal polarizations is completely eliminated independent of frequency. This explains why in Figures 11 and 12 the *VV* and *HH* signals show similar propagation behaviors for all the four measured frequencies. Hence, antenna polarization, as one of the factors controlling radio propagation, plays a more important role for tunnels that have a greater difference between their width and height. The attenuation slopes in Table 2 confirm this finding. For example, at the frequency of 455 MHz, the attenuation slope difference caused by different polarizations is about 21 dB/100 m in Tunnel 1 but is as high as 91 dB/100 m in Tunnel 4.

CONCLUSIONS

Radio propagation in an underground mining environment is generally quite complicated and has not been well understood. In this article, we report a series of propagation measurements in a variety of mines and tunnels. We start with a relatively simple case of a straight, concrete tunnel with smooth walls and show that the propagation behavior in such an environment can be modeled by either the ray-tracing or modal methods. The mines reported include a hard-rock mine with similar horizontal and vertical dimensions, a typical wide eastern coal mine, and a coal mine with a high roof. The measurement results presented in this article provide significant insight into the parameters controlling propagation: tunnel dimensions, frequency, polarization, and electrical properties of tunnel walls. The significance of those controlling factors has also been discussed. For example, the influence of polarization is found to be negligible for tunnels with similar width and height and for high-frequency signals. However, the polarization effect becomes significant for tunnels with dramatically different cross-sectional dimensions (e.g., for a low ceiling often found in eastern coal mines) and, thus, should be considered in the design and deployment of communication systems in these environments.

Extensive measurements have been made in concrete tunnels, coal mines with rock dust and shotcrete, with and without conductive mesh, and hard-rock mines.

DISCLAIMER

The findings and conclusions in this article are ours and do not necessarily represent the views of the National Institute for Occupational Safety and Health (NIOSH). Mention of any company name or product does not constitute endorsement by NIOSH.

AUTHOR INFORMATION

Chenming Zhou received his Ph.D. degree in electrical engineering from Tennessee Technological University in 2008. He is a senior research engineer with the National Institute for Occupational Safety and Health (NIOSH), part of the Centers for Disease Control and Prevention, under the U.S. Department of Health and Human Services. He is currently the project leader and principle investigator for the wireless communications and tracking project at NIOSH. He also serves as a government contract officer representative for NIOSH Broad Agency Announcement contracts related to communications and tracking. Prior to joining NIOSH in August 2012, he was a research fellow at Disney Research Laboratory in Pittsburgh, Pennsylvania, where he conducted research in radio-frequency (RF) ranging based on passive RF identification tags. Before he started his career in industry at Disney, he was a project research scientist with the Department of Electrical and Computer Engineering at Carnegie Mellon University. He holds two U.S. patents in RFID and is the author or coauthor of more than 30 papers published in peer-reviewed journals or conference proceedings.

Timothy Plass received his bachelor's degree in electrical engineering from the University of California, Davis, in 1979, and his master's degree in electrical engineering from Stanford University in 1981. He has held numerous radio-frequency (RF) manufacturing and design positions with Hewlett-Packard, Argo-Systems, Agilent Technologies, General Dynamics, and Boeing designing radios, cell phone test equipment, and antennas. He was an associate fellow with the National Institute for Occupational Safety and Health from 2010 to 2012, where he conducted research on radio propagation in tunnels and coal mines. He is currently a senior RF design engineer with Smith Microwave developing RF surge protection equipment using high-frequency structure simulator simulation. He is a Member of the IEEE.

Ronald Jacksha works for the National Institute for Occupational Safety and Health (NIOSH) Office of Mine Safety and Health Research providing electronic system technical support for wireless communications and tracking research. He was responsible for the development of the test system and methods used in the agency's radio frequency propagation research. Prior to joining NIOSH, he spent 25 years with Hewlett-Packard, then Agilent Technologies, developing wireless communications test systems. In his time with Hewlett-Packard and Agilent Technologies, he gained vast experience in all aspects of electronics from the component level to system design and integration.

Joseph A. Waynert is a retired team leader of the Electrical System Safety and Communications team at the National Institute for Occupational Safety and Health (NIOSH). He is presently a senior consultant to NIOSH through URS Corporation. His primary research focuses on wireless communications and electronic tracking. In particular, he is experimentally and theoretically investigating the mechanisms controlling path loss in underground coal mining applications. System frequency bands of interest include extremely low frequency, medium frequency, and utrahigh frequency. Prior to NIOSH, he worked in industry investigating methods of improved spectrum management for the military. Before that, he worked at Los Alamos National Laboratory developing applications of applied superconductors.

REFERENCES

[1] "Mine improvement and new emergency response act of 2006 (MINER Act)," United States Dept. Labor, United States Public Laws, Arlington, VA, 2006, PL 109–236.

[2] C. L. Colburn, C. M. Bouton, and H. B. Freeman, "Experiments in underground signalling with radio sets," U.S. Bureau of Mines Report of Investigation, Tech. Rep. 2407, Oct. 1922.

[3] R. A. Farmer and N. H. Shepherd, "Guided radiation…The key to tunnel talking," *IEEE Trans. Veh. Commun.*, vol. 14, pp. 93–102, Mar. 1965.

[4] D. G. Dudley, M. Lienard, S. F. Mahmoud, and P. Degauque, "Wireless propagation in tunnels," *IEEE Antennas Propagat. Mag.*, vol. 49, pp. 11–26, Apr. 2007.

[5] T. S. Wang and C. F. Yang, "Simulations and measurements of wave propagations in curved road tunnels for signals from GSM base stations," *IEEE Trans. Antennas Propag.*, vol. 54, pp. 2577–2584, Sept. 2006.

[6] D. Didascalou, R. Maurer, and W. Wiesbeck, "Subway tunnel guided electromagnetic wave propagation at mobile communications frequencies," *IEEE Trans. Antennas Propag.*, vol. 49, pp. 1590–1596, Nov. 2001.

[7] E. Masson, Y. Cocheril, P. Combeau, L. Aveneau, M. Berbineau, R. Vauzelle, and E. Fayt, "Radio wave propagation in curved rectangular tunnels at 5.8 GHz for metro applications, simulations and measurements," *EURASIP J. Wireless Commun. Netw.*, vol. 2011, no. 1, pp. 1–8, 2011.

[8] B. Jacard and O. Maldonado, "Microwave modeling of rectangular tunnels," *IEEE Trans. Microwave Theory Tech.*, vol. 32, no. 6. pp. 576–581, 1984.

[9] Y. Yamaguchi, T. Abe, and T. Sekiguchi, "Radio wave propagation loss in the VHF to microwave region due to vehicles in tunnels," *IEEE Trans. Electromagn. Compat.*, vol. 31, no. 1, pp. 87–91, 1989.

[10] A. E. Goddard, "Radio propagation measurements in coal mines at UHF and VHF," in *Proc. Through-the-Earth Electromagnetics Workshop*, Golden, CO, 1973.

[11] A. Emslie, R. Lagace, and P. Strong, "Theory of the propagation of UHF radio waves in coal mine tunnels," *IEEE Trans. Antennas Propag.*, vol. 23, no. 2, pp. 192–205, 1975.

[12] J. Lee and H. L. Bertoni, "Coupling at cross, T, and L junctions in tunnels and urban street canyons," *IEEE Trans. Antennas Propag.*, vol. 51, pp. 926–935, May 2003.

[13] R. L. Lagace and A. G. Emslie, "Propagation of UHF radio waves in limestone room and pillar mines," U.S. Department of the Interior Bureau of Mines, Washington, DC, Tech. Rep. 387217, 1979.

[14] R. Isberg and R. Chufo, "Passive reflectors as a means for extending UHF signals down intersecting cross cuts in mines or large corridors," in *Proc. 28th Vehicular Technology Conf.*, 1978, pp. 267–272.

[15] Y. P. Zhang, G. X. Zheng, and J. H. Sheng, "Radio propagation at 900 MHz in underground coal mines," *IEEE Trans. Antennas Propag.*, vol. 49, pp. 757–762, May 2001.

[16] M. Lienard and P. Degauque, "Natural wave propagation in mine environments," *IEEE Trans. Antennas Propag.*, vol. 48, pp. 1326–1339, Sept. 2000.

[17] M. Boutin, A. Benzakour, C. Despins, and S. Affes, "Characterization and modeling of a wireless channel at 2.4 and 5.8 GHz in underground tunnels," in *Proc. 3rd Int. Symp. Wireless Communication Systems*, 2006, pp. 517–521.

[18] M. Boutin, A. Benzakour, C. L. Despins, and S. Affes, "Radio wave characterization and modeling in underground mine tunnels," *IEEE Trans. Antennas Propag.*, vol. 56, pp. 540–549, Feb. 2008.

[19] C. Nerguizian, C. L. Despins, S. Affes, and M. Djadel, "Radio-channel characterization of an underground mine at 2.4 GHz," *IEEE Trans. Wireless Commun.*, vol. 4, pp. 2441–2453, Sept. 2005.

[20] M. Ndoh, G. Y. Delisle, and R. Le, "An approach to propagation prediction in a complex mine environment," in *Proc. ICECOM Conf.*, 2003, pp. 237–240.

[21] M. Rak and P. Pechac, "UHF propagation in caves and subterranean galleries," *IEEE Trans. Antennas Propag.*, vol. 55, no. 4, pp. 1134–1138, 2007.

[22] K. A. Remley, G. Koepke, D. G. Camell, C. Grosvenor, G. Hough, and R. T. Johnk, "Wireless communications in tunnels for urban search and rescue robots," in *Proc. 8th Workshop Performance Metrics Intelligent Systems*, 2008, pp. 236–243.

[23] J. Chiba, T. Inaba, Y. Kuwamoto, O. Banno, and R. Sato, "Radio communication in tunnels," *IEEE Trans. Microwave Theory Tech.*, vol. 26, no. 6, pp. 439–443, 1978.

[24] Y. P. Zhang, Z. R. Jiang, T. S. Ng, and J. H. Sheng, "Measurements of the propagation of UHF radio waves on an underground railway train," *IEEE Trans. Veh. Technol.*, vol. 49, pp. 1342–1347, July 2000.

[25] J. M. Molina-Garcia-Pardo, M. Lienard, A. Nasr, and P. Degauque, "On the possibility of interpreting field variations and polarization in arched tunnels using a model for propagation in rectangular or circular tunnels," *IEEE Trans. Antennas Propag.*, vol. 56, pp. 1206–1211, Apr. 2008.

[26] E. Masson, P. Combeau, M. Berbineau, R. Vauzelle, and Y. Pousset, "Radio wave propagation in arched cross section tunnels—simulations and measurements," *J. Commun.*, vol. 4, no. 4, pp. 276–283, 2009.

[27] C. Zhou, J. Waynert, T. Plass, and R. Jacksha, "Modeling RF propagation in tunnels," in *Proc. IEEE Int. Symp. Antennas Propagation*, Orlando, FL, 2013, pp. 1916–1917.

[28] C. Zhou, J. Waynert, T. Plass, and R. Jacksha, "Attenuation constants of radio waves in lossy-walled rectangular waveguides," *Progr. Electromagn. Res.*, vol. 142, pp. 75–105, 2013.

[29] S. F. Mahmoud and J. R. Wait, "Geometrical optical approach for electromagnetic wave propagation in rectangular mine tunnels," *Radio Sci.*, vol. 9, no. 12, pp. 1147–1158, 1974.

[30] Z. Sun and I. F. Akyildiz, "Channel modeling and analysis for wireless networks in underground mines and road tunnels," *IEEE Trans. Commun.*, vol. 58, pp. 1758–1768, June 2010.

[31] C. Zhou and J. Waynert, "The equivalence of the ray tracing and modal methods for modeling radio propagation in tunnels," *IEEE Antennas Wireless Propagat. Lett.*, vol. 13, pp. 615–618, Mar. 2014.

[32] K. D. Laakmann and W. H. Steier, "Waveguides: Characteristic models of hollow rectangular dielectric waveguides," *Appl. Opt.*, vol. 15, pp. 1334–1340, May 1976.

[33] L. B. Felsen, F. Akleman, and L. Sevgi, "Wave propagation inside a two-dimensional perfectly conducting parallel-plate waveguide: Hybrid ray-mode techniques and their visualizations," *IEEE Antennas Propagat. Mag.*, vol. 46, pp. 69–89, Dec. 2004.

[34] R. E. Collin, *Field Theory of Guided Waves*, vol. 2. New York: IEEE Press, 1991.

[35] J. Alonso, B. Izquierdo, and J. Romeu, "Break point analysis and modelling in subway tunnels," in *Proc. 3rd European Conf. Antennas Propagation*, 2009, vols. 1–6, pp. 3138–3142.

[36] K. Guan, Z. Zhong, B. Ai, and C. Briso-Rodríguez, "Research of propagation characteristics of break point: Near zone and far zone under operational subway condition," in *Proc. 6th Int. Wireless Communications Mobile Computing Conf.*, Caen, France, 2010, pp. 114–118.

[37] Y. P. Zhang, "Enhancement of waveguide model for propagation-loss prediction in tunnels," *Microw. Opt Technol. Lett.*, vol. 30, pp. 10–12, July 5, 2001.

[38] T. Klemenschits and E. Bonek, "Radio coverage of road tunnels at 900 and 1800 MHz by discrete antennas," in *Proc. 5th IEEE Int. Symp. Personal, Indoor Mobile Radio Communications*, The Hague, The Netherlands, 1994, pp. 411–415.

[39] R. Martelly and R. Janaswamy, "An ADI-PE approach for modeling radio transmission loss in tunnels," *IEEE Trans. Antennas Propag.*, vol. 57, pp. 1759–1770, June 2009.